Am J Physiol Heart Circ Physiol 323: H628–H639, 2022.
First published August 19, 2022; doi:10.1152/ajpheart.00208.2022

american physiological society

AMERICAN JOURNAL OF PHYSIOLOGY
HEART AND CIRCULATORY PHYSIOLOGY

INNOVATIVE METHODOLOGY

Innovation in Improving Rigor and Reproducibility in Cardiovascular Research

Fully automated mouse echocardiography analysis using deep convolutional neural networks

Chong Duan,[1] Mary Kate Montgomery,[2] Xian Chen,[2] Soumya Ullas,[2] John Stansfield,[1] Kevin McElhanon,[3] and Dinesh Hirenallur-Shanthappa[2]

[1]*Early Clinical Development, Pfizer Incorporated, Cambridge, Massachusetts;* [2]*Comparative Medicine, Pfizer Incorporated, Cambridge, Massachusetts; and* [3]*Rare Disease Research Unit, Pfizer Incorporated, Cambridge, Massachusetts*

Abstract

Echocardiography (echo) is a translationally relevant ultrasound imaging modality widely used to assess cardiac structure and function in preclinical models of heart failure (HF) during research and drug development. Although echo is a very valuable tool, the image analysis is a time-consuming, resource-demanding process, and is susceptible to interreader variability. Recent advancements in deep learning have enabled researchers to automate image processing and reduce analysis time and interreader variability in the field of medical imaging. In the present study, we developed a fully automated tool, mouse-echocardiography neural net (MENN), for the analysis of both long-axis brightness (B)-mode and short-axis motion (M)-mode images of left ventricle. MENN is a series of fully convolutional neural networks that were trained and validated using manually segmented B-mode and M-mode echo images of the left ventricle. The segmented images were then used to compute cardiac structural and functional metrics. The performance of MENN was further validated in two preclinical models of HF. MENN achieved excellent correlations (Pearson's r = 0.85–0.99) and good-to-excellent agreement between automated and manual analyses. Further interreader variability analysis showed that MENN has better agreements with an expert analyst than both a trained analyst and a novice. Notably, the use of MENN reduced manual analysis time by >92%. In conclusion, we developed an automated echocardiography analysis tool that allows for fast and accurate analysis of B-mode and M-mode mouse echo data and mitigates the issue of interreader variability in manual analysis.

NEW & NOTEWORTHY Echocardiography is commonly used in preclinical research to evaluate cardiac structure and function. Despite the broad applications across therapeutic areas, the analysis of echo data is laborious and susceptible to interreader variability. In this study, we developed a fully automated mouse-echocardiography neural net (MENN). Cardiac measurements from MENN showed excellent correlations with manual analysis. Furthermore, the use of MENN leads to >92% reduction in analysis time and potentially eliminates the interobserver variability issue.

automated image analysis; deep learning; echocardiography; heart failure; preclinical imaging

INTRODUCTION

Echocardiography (echo), an ultrasound-based noninvasive imaging approach, is widely used as a diagnostic tool in the clinic, as well as in preclinical research to assess cardiac structure and function in animal models (1, 2). In preclinical drug discovery, this imaging modality is routinely used to assess cardiac disease burden in animal models of heart failure and to assess the cardiovascular safety of new drugs (1). It is a high-throughput imaging modality that is accurate, reproducible, easy to use, and affordable compared with other imaging modalities such as cardiac magnetic resonance imaging, computed tomography, or myocardial scintigraphy (3). Although recent advancements in echocardiography imaging have enabled clinicians to acquire cardiac images in three dimensions and have improved the accuracy of cardiac structural and functional readouts (4), two-dimensional echocardiography (2-D echo) remains the most used technique in preclinical heart failure research and drug development (1, 5).

To obtain reliable and reproducible information from echocardiography that can be used to compare results between different laboratories, one needs to consider several factors, which include type and depth of anesthesia, the mode of recording, and sonographer experience in the analysis of preclinical research (1, 6). Although the type and depth of anesthesia and the mode of recording can be standardized, observed variability due to analyst experience or subjective bias in echo analysis is hard to control and standardize (7). As

Correspondence: D. Hirenallur-Shanthappa (dineshh@pfizer.com).
Submitted 27 April 2022 / Revised 2 August 2022 / Accepted 16 August 2022

a result, it is challenging to compare echo readouts between preclinical laboratories and reproduce data from one laboratory in another. The current workflow of 2-D echo analysis in preclinical research requires manual tracing of endocardial borders at end-systolic and end-diastolic frames using a preset analysis tool/program to compute cardiac functional and structural information. Although manual analysis is a simple process, it is very time and resource-demanding. Its accuracy depends on the analyst's experience, and it is susceptible to analyst bias and interreader variability (8). These drawbacks of echocardiography imaging are not exclusive to preclinical use but also exist in the clinic as well (7).

To address the limitations of manual echo analysis, several clinical echo machine manufacturers have developed algorithms to compute left ventricle (LV) indices on brightness (B)- and motion (M)-mode echocardiography images (9–13). The use of these automated tools in clinical applications has been shown to improve accuracy, reproducibility, and efficiency; thus, these types of tools are slowly being adopted in clinics for echocardiography analysis (10). However, there is no fully automated tool for the analysis of B- and M-mode echocardiography images in preclinical research. Recently, FUJIFILM VisualSonics Vevo LAB, a proprietary preclinical echo analysis tool, released a software version with a semiautomated 2-D border detection algorithm (Auto2DE or AutoLV) for analysis of left ventricle parasternal long-axis (PSLAX) images of B-mode and parasternal short-axis (PSAX) images of M-mode (14, 15). Similarly, VivoQuant, a proprietary image analysis solution, released a semiautomated ultrasound B/M-mode segmentation module for the analysis of mouse echocardiography images (16). Notably, both these proprietary tools require an image analyst's input to perform analysis in their respective analysis tool. For example, an analyst must manually open LV PSLAX B-mode images in the Vevo LAB or the VivoQuant and navigate to the "R" wave on a simultaneously recorded electrocardiogram or select the region of maximum and/or minimum LV dilatation on a cine loop to initiate automated tracing of the left ventricular wall (14, 16). Although use of the Auto2DE or AutoLV and VivoQuant tools significantly reduces left ventricle (LV) wall tracing time, the amount of time an analyst needs to spend on opening each individual echo image and navigating through the cine loop to choose a section of the loop for autotracing is still significant. The semiautomated echo tool does not save much overall time on the manual effort needed for echo analysis. Furthermore, the accuracy of Auto2DE's performance varies widely from model to model, and the correlation of ejection fraction (EF) from the Auto2DE to manual analysis output yields a Pearson's coefficient value of r = 0.33–0.67, depending on the quality of the LV PSLAX B-mode images (14). There is a need for a fully automated echo analysis tool that would significantly reduce manual analysis time, improve accuracy, and eliminate observer variability in preclinical heart failure models. Thus, the aim of this study was to develop and validate a deep learning-based, fully automated echo analysis tool for the analysis of LV PSLAX B-mode and PSAX M-mode echo images of a mouse and to assess the performance of this tool on models of dilated and hypertrophic cardiomyopathy in mice.

METHODS

Animal Models

All procedures involving animals were reviewed and approved by Pfizer's Institutional Animal Care and Use Committee and conducted in an Association for Assessment and Accreditation of Laboratory Animal Care International-accredited facility. Mice [n = 653; male (n = 574) and female (n = 79); age 8–35 wk; genetically engineered mouse models or 129S1/SvlmJ (or C57BL/6NCrl)] were anesthetized using isoflurane (3% for induction, 1%–2% for maintenance) or sevoflurane (6% for induction, 1%–4% for maintenance) for echocardiography image acquisition. Approximately 90%–95% of echo-image acquisition was performed under isoflurane anesthesia, and ~5%–10% of images were acquired under sevoflurane anesthesia. Regardless of the type of anesthesia, heart rate was maintained between ~400 and 550 beats/min during image acquisition. The method development and validation work included echocardiography images from a wide variety of disease models including transverse aortic constriction (TAC), angiotensin II-induced, renin overexpression plus N^G-nitro-L-arginine methyl ester-induced, high-fat diet-induced obesity (DIO), and genetic-engineered models (GEMs) of heart failure (Supplemental Table S1; all Supplemental material is available at https://doi.org/10.6084/m9.figshare.20412552.v1).

Echocardiography Data

PSLAX B-mode and PSAX M-mode echocardiography images of the murine left ventricle were taken either using MX250S/MS-250S (center frequency, 21 MHz; frequency band, 15–30 MHz; and axial resolution, 75 μm) or MX550D/MS-550S (center frequency, 40 MHz; frequency band, 25–55 MHz; and axial resolution, 40 μm) with a VisualSonics Vevo 3100 or Vevo 2100 ultrasound machine (FUJIFILM VisualSonics, Toronto, Canada) and exported from VisualSonics' Vevo LAB software in DICOM format. B-mode images consisted of 300 frames capturing the left ventricle in motion (2-D + time). M-mode images consisted of 2–5 s of cross-sectional snapshots (1-D + time) broken up into 10–40 frames.

Manual segmentation of the left ventricle was performed by an expert analyst on 586 B-mode videos (33,133 frames) and 976 M-mode images in FUJIFILM VisualSonics Vevo LAB software. The boundary around the left ventricle was manually drawn on the B-mode videos for two to six cardiac cycles, and the software interpolated the boundary for the remaining slices. The edges of the anterior and posterior wall were manually drawn on the M-mode images for a single frame capturing ~1 s of M-mode acquisition. From these segmentations, many metrics were calculated including LV end-systolic and -diastolic area (LVESA; LVEDA), LV end-systolic and -diastolic volume (LVESV; LVEDV), and ejection fraction (EF) for B-mode, and LV posterior and anterior wall thickness at systole and diastole, LV mass, fractional shortening (FS), and heart rate for M-mode.

Both B-mode and M-mode scans were exported in DICOM format from the Vevo LAB software as described earlier and cropped down to remove annotations so that only the B-mode or M-mode image itself remained. For the ground-

truth training data, the annotated images were then parsed automatically to compute a segmentation label that could be used for comparison with the automated result.

Segmentation of LV and Myocardial Wall

In the present study, a U-Net architecture (17) was repurposed to segment the left ventricle and myocardial wall on both B-mode and M-mode images. Specifically, the B-mode segmentation network was trained to perform a binary classification of every single B-mode frame into background and left ventricle. B-mode frames (33,133) with manual annotations were randomly split into a training (80%) set and a testing (20%) set. Training was performed with a dice similarity coefficient (DSC)-based loss function and an Adam optimizer, using a batch size of 32 over 100 epochs or until early stopping criteria was met. The 20% testing set was used independently to obtain the dice scores. The early stopping criteria is defined as when the DSC-based loss is no longer decreasing for 10 consecutive epochs. The DSC is defined as following:

$$\mathrm{DSC} = \frac{2 \times |A \cap B|}{|A| + |B|}$$

where $|A|$ represents the area of manual segmentation, $|B|$ represents the area of auto segmentation, and $|A \cap B|$ represents the comment area between the two segmentations. The following parameters were used for the training optimizer: learning rate = 0.0001, $\beta_1 = 0.9$, $\beta_2 = 0.999$, and $\varepsilon = 0.0000001$.

For M-mode, the segmentation network was trained in a similar manner to the B-mode with a few exceptions. In this case, a multiclass segmentation version of a U-Net was trained to segment a single M-mode frame into background, anterior wall, left ventricle interior, and posterior wall. Training was performed on 976 M-mode images with an 80/20 train-test split over 100 epochs or until stopping criteria was met. The trained networks for both B-mode and M-mode were subsequently further validated using two independent data sets [the hypertrophic cardiomyopathy (HCM) and dilated cardiomyopathy (DCM) data sets as defined in the below section]. Performance was evaluated using dice similarity coefficient and correlation of calculated LV metrics to manual analysis. All model training and testing were done in Python using the TensorFlow deep learning library with two NVIDIA GeForce RTX 2080 GPUs and 64 GB RAM. The code for MENN is available at https://github.com/pfizer-opensource/mouse-echo-neural-net.

LV Metrics Quantification

For B-mode, LV area was first computed from the segmentation mask and the in-plane resolution (0.015–0.018 mm). Often, the quality of ECG signals acquired during mouse echo acquisition is poor. Thus, instead of relying on an ECG signal to detect LV systolic and diastolic frames, the maximum and minimum LV area from the segmentation masks were used to determine diastolic and systolic frames, respectively. The LV area and length of the LV long axis were computed throughout a cine loop over multiple cardiac cycles, which eliminated interbeat variability issue. LV volumes (V) were then calculated using the single-plane area-length method (18, 19):

$$\mathrm{V} = \frac{8}{3}\pi \times A^2/L$$

in which A is the LV area and L is the LV long-axis length measured as the line from the LV apex to the mitral valve annulus. Systolic and diastolic cardiac phases were detected based on a Gaussian-smoothed LV area-time curve, and end-diastolic volume (LVEDV) and end-systolic volume (LVESV) were calculated accordingly. EF was calculated using the average EDV and ESV across the entire B-mode video clip as follows:

$$\mathrm{EF} = \frac{\mathrm{EDV} - \mathrm{ESV}}{\mathrm{EDV}} \times 100\%.$$

For M-mode, systolic and diastolic phases were first detected based on the segmentation mask as shown in Fig. 1. Both anterior and posterior LV wall thicknesses at end-systolic and -diastolic phases were then computed as the vertical distance between the region boundary lines from the segmentation mask. The vertical pixel resolution on M-mode images ranges from 0.026 to 0.028 mm. Fractional shortening (FS) and the corrected LV mass (in mg) were computed as follows (20, 21):

$$\mathrm{LV\ mass} = 1.503 \times [(\mathrm{LVID;d} + \mathrm{LVPW;d} + \mathrm{IVS;d})^3 - \mathrm{LVID;d}^3,$$

$$\mathrm{LV\ mass\ corrected} = 0.8 \times \mathrm{LV\ mass}$$

in which LVID;d is LV diameter at diastole, LVPW;d is the posterior LV wall thickness at diastole, and IVS;d is the anterior LV wall thickness at diastole and

$$\mathrm{FS} = \left(\frac{\mathrm{LVID;d} - \mathrm{LVID;s}}{\mathrm{LVID;d}}\right) \times 100\%$$

where LVID;d is LV diameter at diastole and LVID;s is LV diameter at systole.

Deployment

For front-end use, a simple graphical user interface was designed in Python's Tkinter toolbox to take as an input a folder path containing both B-mode and M-mode DICOMs. Mouse-echo neural net (MENN) then parsed B-mode and M-mode images, fed each into their respective model for segmentation, and saved a .csv of the various metrics calculated from the segmentation of each image, as well as a .pdf containing snapshots of the automated segmentations for quality control (QC) purposes. A schematic representation of the automated analysis workflow can be found in Supplemental Fig. S2.

Performance of the Automated Analysis Tool on Heart Failure Models

Regardless of disease etiology and induction method, most preclinical heart failure models show structural change either as dilated cardiomyopathy or hypertrophic cardiomyopathy. Thus, the performance of the fully automated echo analysis tool was assessed on genetically engineered mouse models of dilated cardiomyopathy (DCM) and hypertrophic cardiomyopathy (HCM). The cardiac-specific B-cell lymphoma (BCL)-2-associated athanogene (BAG3) knockout

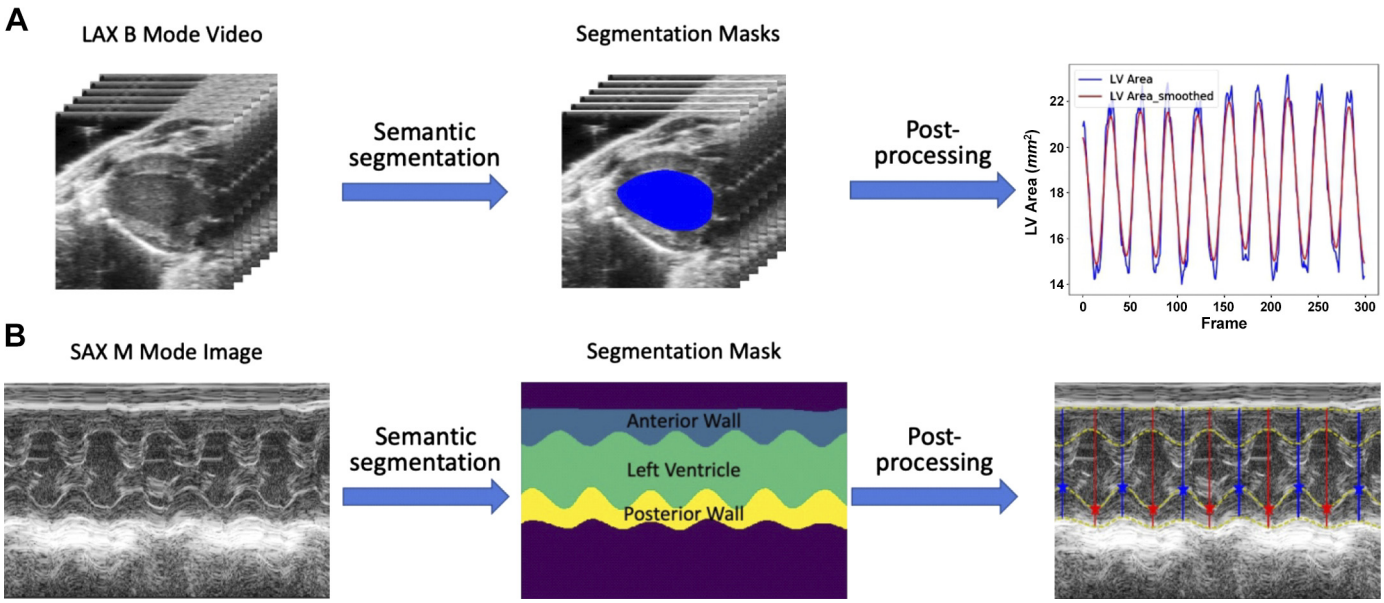

Figure 1. Echo analysis workflow. *A*: for each long-axis B-mode echo video, semantic segmentations were performed for each frame using a convolutional neural network. The segmentation results were then processed to obtain left ventricle (LV) areas and volumes. The LV area-time curves were then smoothed to identify systolic and diastolic frames, which were used later for the computation of all B-mode cardiac metrics. *B*: for each short-axis M-mode image, semantic segmentation was performed to identify four regions: background (purple), anterior wall (blue), left ventricle (green), and posterior wall (yellow). Postprocessing was then applied to the segmentation mask image to identify region boundaries and detect systolic and diastolic phases. echo, echocardiography; LAX B mode, long-axis brightness-mode; SAX M mode, short-axis motion-mode.

animals show an age-dependent decline in cardiac function and left ventricular dilatation (22). Thus, for the evaluation of performance of the tool on a DCM model, LV PSLAX B-mode (n = 102) and PSAX M-mode echo images (n = 100) from a mixed cohort of cardiac-specific BCL-2-associated athanogene (BAG3) knockout (70%) and littermate control (30%) animals were used to compare key echo readouts (EF, FS, LVESV, and LVEDV) between the MENN output and manual analysis. The cardiac-specific myosin-binding protein-C (MYBP-C) knockout animals show a severe cardiac hypertrophy phenotype with increased LV wall thickness (23). For the evaluation of the performance of MENN on an HCM model, LV PSLAX B-mode images (n = 103) and PSAX M-mode images (n = 98) from a mixed cohort of MYBP-C3 knockout (45% KO) and littermate or background strain control animals (55%) were used to compare key echo readouts [EF, FS, left ventricle anterior wall thickness (LVAW), left ventricle posterior wall thickness (LVPW), and LV mass corrected] between the automatedanalysis output and manual analysis.

Statistical Analysis

Statistical analysis was performed using Graph Prism 9 (Graph Pad Software, La Jolla, CA). Normality of the echo variables was evaluated using a Shapiro–Wilk test and a quantile-quantile (QQ) plot. All variables are normally distributed or approximately normally distributed (see QQ plots in Supplemental Fig. S1). For each echo readout, the comparison between automated and manual outputs included linear regression with Pearson correlation coefficients and Bland–Altman analyses to assess the bias and limits of agreement (defined as means ± 2SD). In addition, consistency and agreement between various echo readouts were compared using intraclass correlation (ICC).

RESULTS

Semantic Segmentation

Deep convolutional neural networks were used to perform semantic segmentations on both B-mode and M-mode images. For B-mode, MENN was evaluated on a test set of 7,015 frames or 117 B-mode videos. Figure 2 shows a direct comparison between the deep learning model's automated segmentations (green) and an expert user's manual segmentations (red) of the left ventricle in several representative B-mode frames. Overall, when comparing with the manual segmentation done by a subject matter expert (SME), the dice index is 0.9245. Similarly, MENN was compared against manual segmentation on a test set of 129 M-mode scans. Figure 2*B* shows the direct comparison between the model's automated segmentations (green) and the expert user's manual segmentations (red) for representative scans. Overall, the segmentation had a pixel accuracy for all four regions (background, anterior wall, LV, and posterior wall) for the testing data set of 0.9563.

Comparison of LV Metrics

Following the segmentations, LV metrics were computed for both B-mode and M-mode data. The LV metrics, including EF, LVESV, LVEDV, LVESA, and LVEDA, computed on B-mode images, showed excellent correlation (Pearson's r ranges from 0.93 to 0.98) between automated and manual analysis (Fig. 3). Furthermore, Bland–Altman analysis showed good agreement between auto and manual EF, LVESV, LVEDV, LVESA, and LVEDA with bias of −4.69, 1.02, −3.10, 0.47, and −0.70, respectively.

Similarly, the comparison of LV metrics such as fractional shortening (FS), posterior LV wall thickness at systole

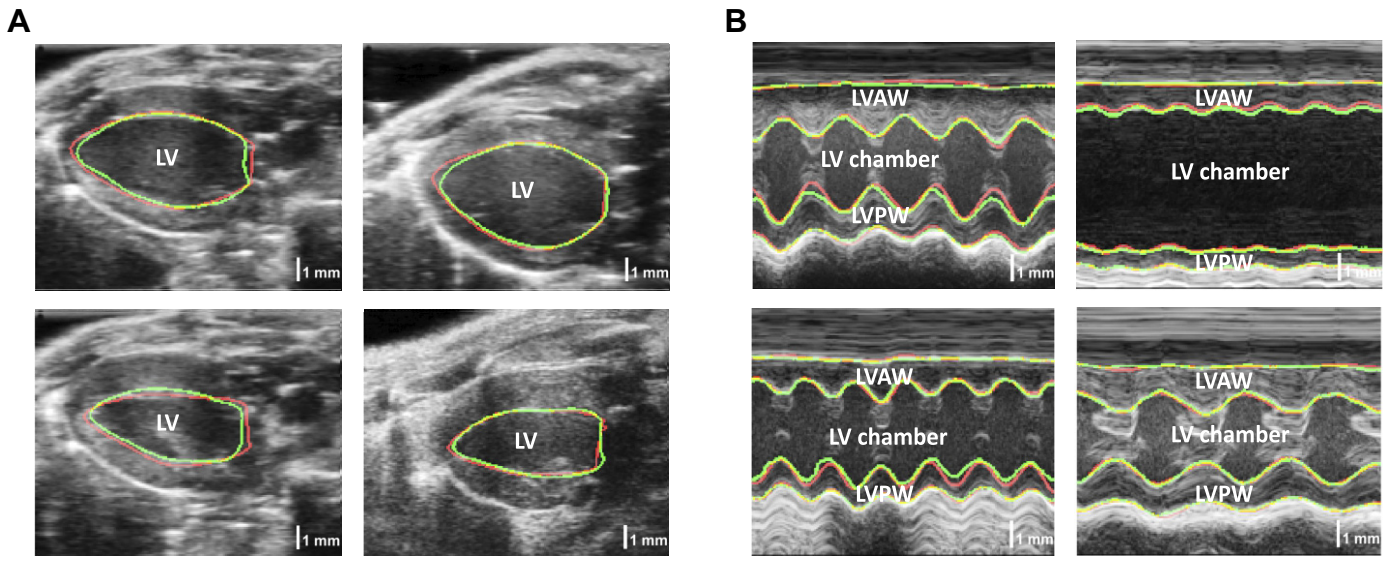

Figure 2. Representative B-mode (*A*) and M-mode (*B*) images of left ventricle (LV) with manual (red) and automated (green) tracing of the internal LV wall (B-mode) and the anterior, internal, and posterior walls (M-mode). Yellow pixels indicate an overlap in the manual and automated segmentations. B mode, brightness-mode; LVAW, left ventricle anterior wall thickness; LVPW, left ventricle posterior wall thickness; M mode, motion-mode.

(LVPWs), posterior LV wall thickness at diastole (LVPWd), anterior LV wall thickness at systole (LVAWs), anterior LV wall thickness at diastole (LVAWd), and corrected LV mass computed from M-mode images showed excellent correlation between the automated and manual segmentation outputs (Fig. 4). The Bland–Altman analysis showed good agreement between auto and manual FS, LVPWs, LVPWd, LVAWs, LVAWd, and LV mass corrected with bias of 3.85, −0.70, −0.01, −0.04, −0.01, and −4.73, respectively (Fig. 4). Note that, in general, M-mode-binding measurements are considered less reliable than B-mode-based measurements.

Evaluation of the MENN Tool in Heart Failure Models

The MENN echo analysis tool was then further tested with data collected from two heart failure models: DCM and HCM. The data from mixed cohort of the DCM model (Fig. 5) showed an excellent correlation between MENN and manual analysis done by an expert (Pearson's r = 0.93, 0.91, 0.99, and 0.97, respectively) for LV ejection fraction (LVEF), FS, LVESV, and LVEDV. Bland–Altman analysis revealed a bias of −7.5 ± 4.1 for LVESV, −11.4 ± 5.7 for LVEDV, and −13.6 ± 6.2 for FS, suggesting consistent underestimation of LV volumes and FS by MENN compared with manual analysis (Fig. 5). However, despite the negative biases, the strong correlation for EF and FS between MENN and manual analysis suggests that this underestimation of absolute volume will not significantly affect the assessment of systolic function. Similarly, the data from a mixed cohort of the HCM model (Fig. 6) demonstrated a good correlation between MENN and manual analysis performed by an SME for LVEF, FS, and corrected LV mass (Pearson's r = 0.80, 0.91, and 0.97 respectively). As with the DCM model, the Bland–Altman analysis revealed a bias of −11.28 ± 7.2 for FS in HCM models, suggesting consistent underestimation of FS with MENN compared with manual analysis. Although the absolute FS values do not match perfectly, the correlation was excellent between MENN and manual analysis, again suggesting that the underestimation of absolute FS did not affect the assessment of cardiac function in this model.

Analysis Efficiency and Interobserver Variability

To evaluate the time saved by using MENN, the time required to analyze a sample data set containing PSLAX B- and PSAX M-mode images of the LV of 32 mice (normal, HCM, and DCM) and report the data were compared between MENN, an expert, a trained analyst, and a novice. The average time required to perform manual analysis of both PSLAX B- and PSAX M-mode LV images and report results was 5.27 min/animal for an expert, and 8.33 min/animal for a trained analyst. Meanwhile, it took less than 0.4 min/animal for MENN (potential QC time considered). Notably, there was no manual supervision needed during MENN analysis. Overall, more than 92% less time was required for the analysis of echo images from a single animal per time point compared with the time required by an expert for analysis.

In addition to increased efficiency in echocardiography analysis, EF data showed far better correlation between MENN and expert analysis compared with expert versus novice or expert versus trained (Fig. 7). The interreader consistency and agreement of EF values are higher between expert analysis and MENN compared with expert versus novice analysis (Table 1). Importantly, the MENN analysis showed no intraobserver variability when analyzing the same images twice. Use of MENN eliminates intra- and interobserver bias from echo analysis. Overall, these results suggest that MENN's analysis output values show excellent agreement with expert analysis.

Image Segmentation Failure Rate

The performance of the MENN tool depended on the quality of the echo image. During the MENN performance analysis, ∼5%–6% of PSLAX B-mode and 10%–11% of PSAX M-mode LV images failed QC because of poor segmentation. These segmentation failures are primarily due to poor image quality,

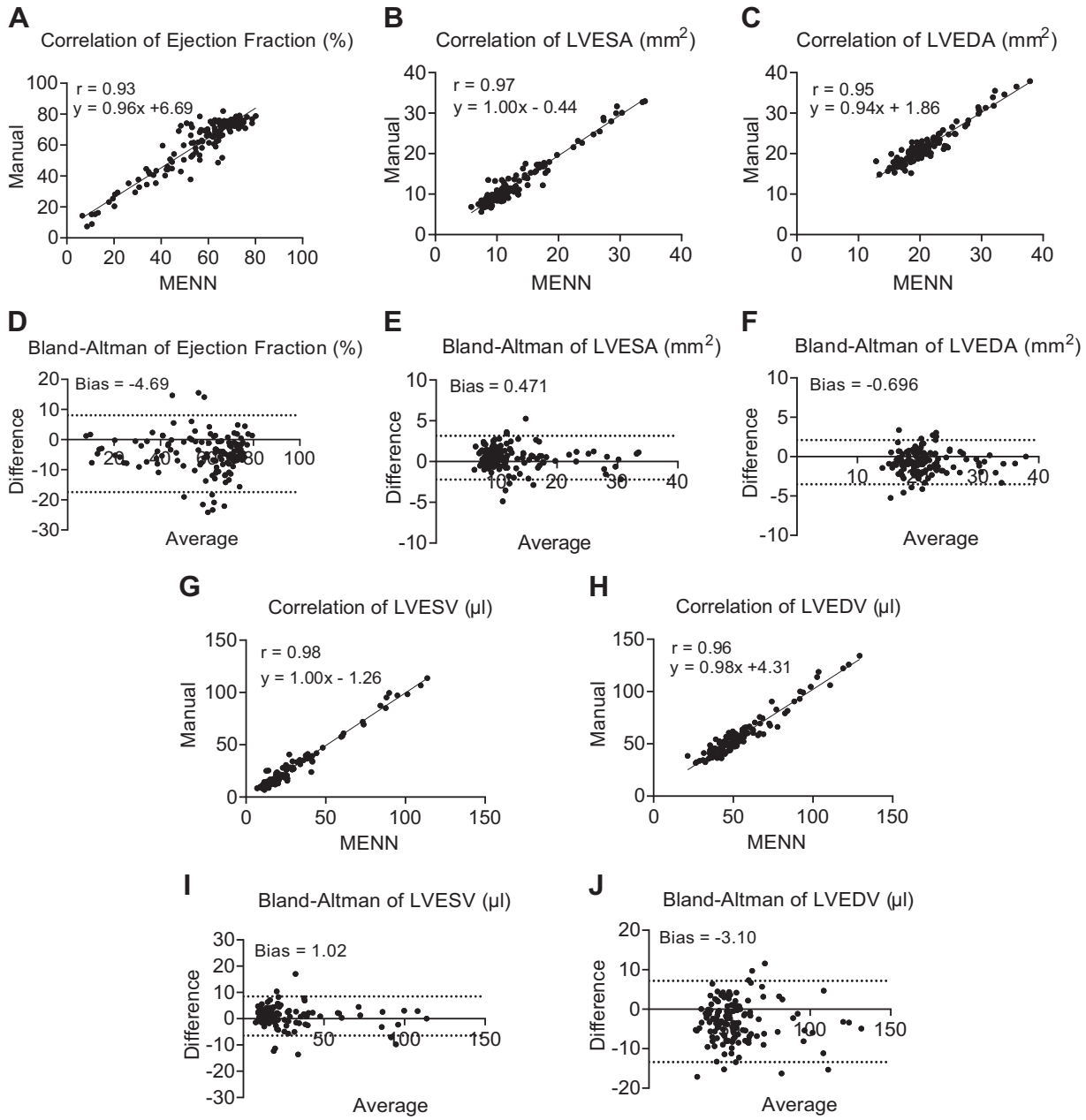

Figure 3. Comparing the mouse-echo neural net against expert manual analysis on left ventricle (LV) indications from long-axis (PSLAX) B-mode images (n = 134). Correlations between the manual user (y-axis) and the automated tool (x-axis) for ejection fraction, LV systolic and diastolic area (LVESA and LVEDA, respectively), and LV systolic and diastolic volume (LVESV and LVEDV, respectively) are shown in *A*, *B*, *C*, *G*, and *H*, respectively. The corresponding Bland–Altman plots are shown in *D*, *E*, *F*, *I*, and *J*, respectively. A simple linear regression line is plotted for each correlation graph, with the equation and correlation value in the *top left* corner, and a 95% confidence interval (CI) is plotted for each Bland–Altman plot, with the bias shown in the *top left* corner. B mode, brightness-mode; echo, echocardiography; LVEDA, LV end-diastolic area; LVEDV, LV end-diastolic volume; LVESA, LV end-systolic area; LVESV, LV end-systolic volume; MENN, mouse-echocardiography neural net; PSLAX, left ventricle parasternal long-axis.

which includes the presence of rib shadowing or motion artifacts, or an improper image acquisition plane (Fig. 8). These results suggest that the quality of echo images is paramount to reduce image segmentation failures and increase the success of the MENN analysis tool's performance.

DISCUSSION

Echocardiography is commonly used in preclinical research to evaluate cardiac structure and function for various cardiovascular disease models including dilated cardiomyopathy and hypertrophic cardiomyopathy. In addition, echo is often used to monitor safety and assess cardiotoxicity in drug research and development. Despite the broad applications across therapeutic areas, the analysis of echo data, which includes outlining heart chambers over a cardiac cycle, is laborious. The manual outlining process is also susceptible to interreader variability. In this study, we developed and validated a fully automated mouse-echocardiography neural net (MENN)

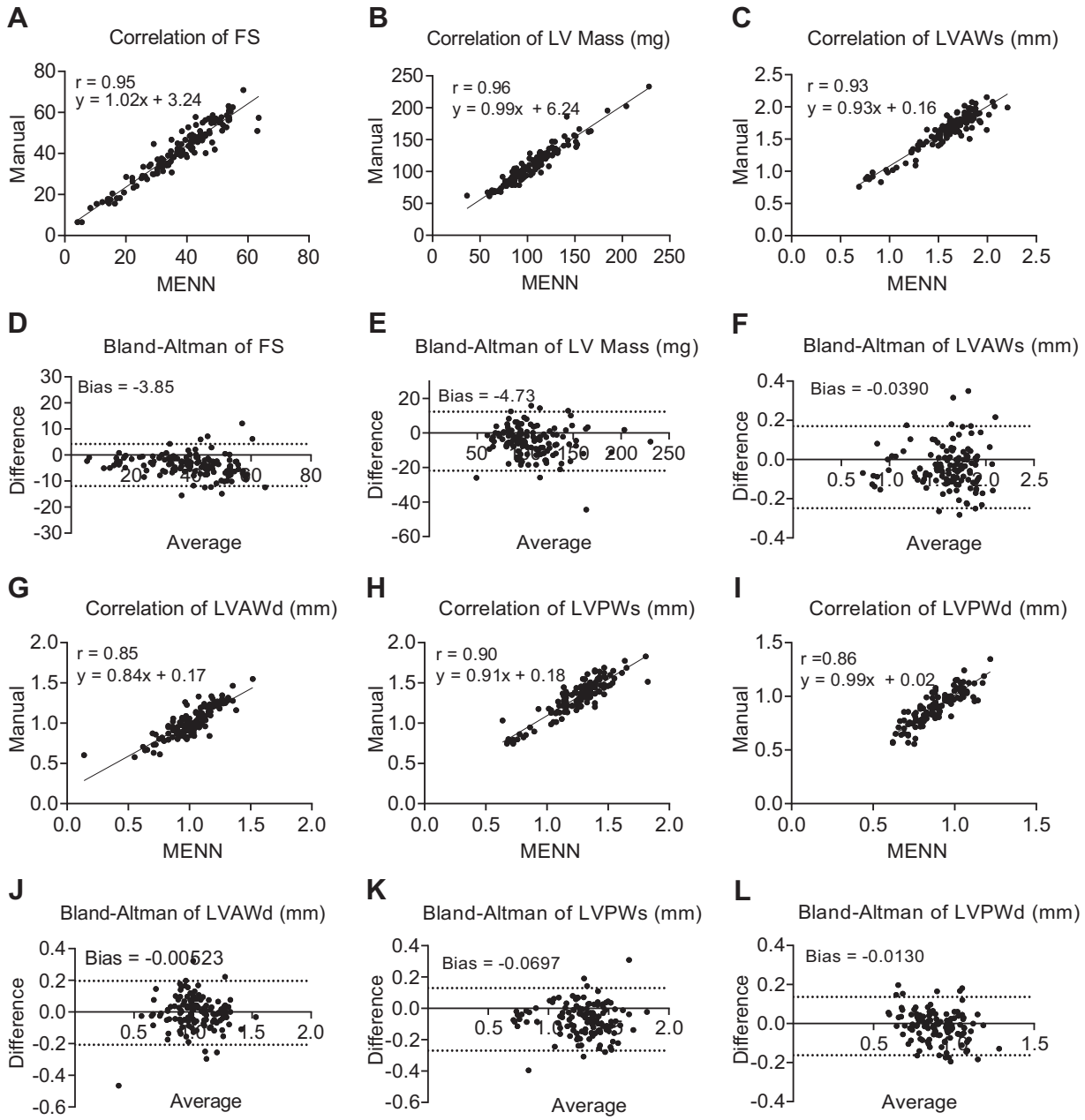

Figure 4. Comparing the mouse-echo neural net against expert manual analysis on left ventricle (LV) indications from short-axis (SAX) M-mode images (n = 128). Correlations between the manual user (y-axis) and the automated tool (x-axis) for fractional shortening, corrected LV mass, systolic and diastolic anterior wall thickness (LVAWs and LVAWd, respectively), and systolic and diastolic posterior wall thickness (LVPWs and LVPWd, respectively) are shown in *A*, *B*, *C*, *G*, *H*, and *I*, respectively. The corresponding Bland–Altman plots are shown in *D*, *E*, *F*, *J*, *K*, and *L*, respectively. A simple linear regression line is plotted for each correlation graph, with the equation and correlation value in the *top left* corner, and a 95% CI is plotted for each Bland–Altman plot, with the bias shown in the *top left* corner. CI, confidence interval; echo, echocardiography; LVAWs, LV wall thickness at diastole; LVPWd, posterior LV wall thickness at diastole; LVPWs, posterior LV wall thickness at systole; MENN, mouse-echocardiography neural net; M mode, motion-mode.

using deep learning. The performance of MENN on both PSLAX B- and PSAX M-mode images from mouse DCM and HCM models showed an excellent correlation between automated output and manual analysis. Furthermore, the use of MENN analysis showed more than 92% reduction in echocardiography analysis time and potentially eliminated the concern of intraobserver and interobserver variability.

Deep learning models have been increasingly used for medical image analysis in both the research setting and the clinic (24–27). In the clinical cardiovascular imaging space, there has been a surge in successful deep learning applications thanks to the availability of large numbers of images with annotations. This is particularly true for echocardiography since it is often the first-line imaging modality used for assessing cardiovascular disease due to its low cost and wide availability. For example, Madani et al. (28) developed a convolutional neural network to classify transthoracic echocardiogram views as this is often the first step toward

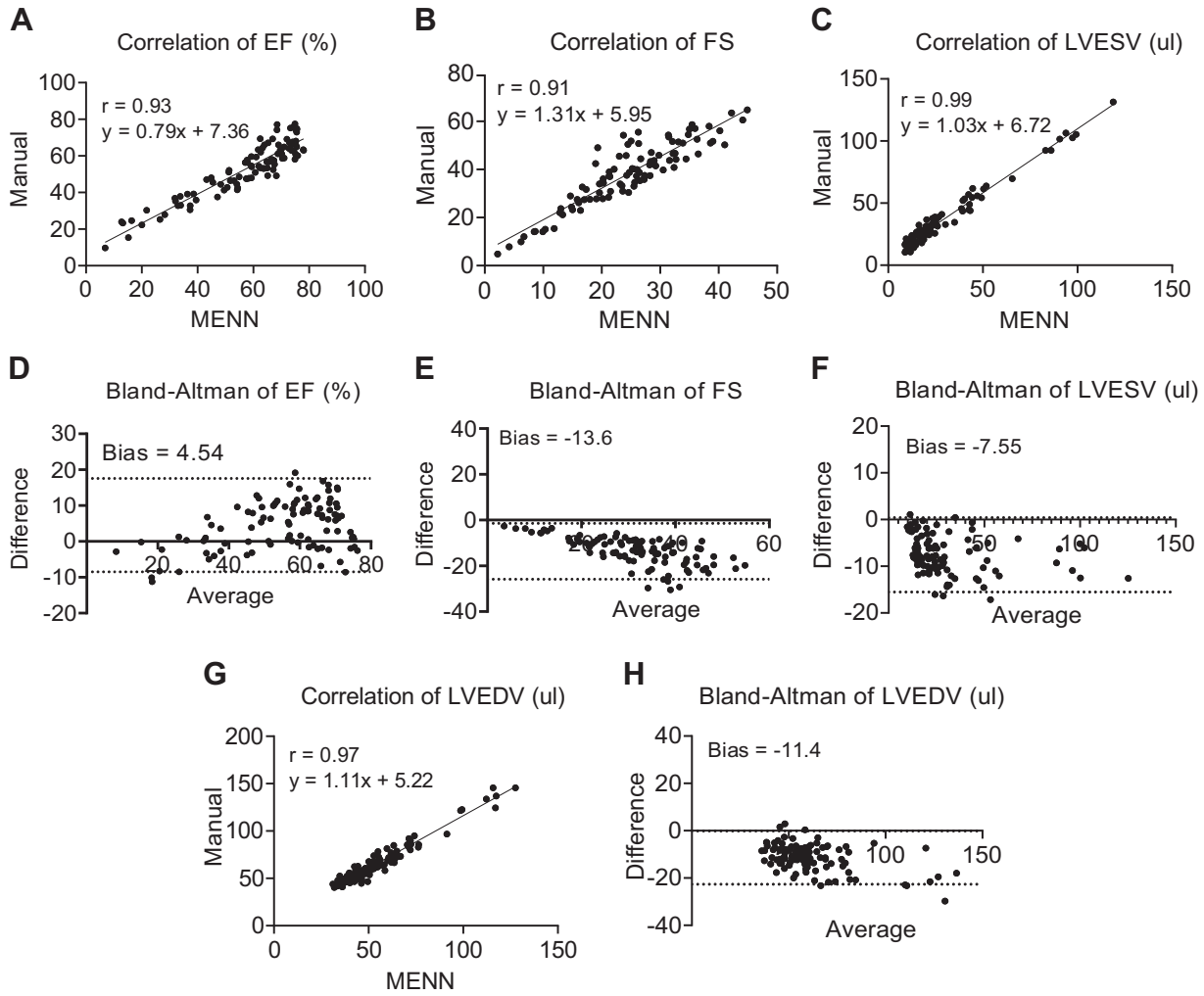

Figure 5. Performance of the mouse-echo neural net on echo images taken from the mixed cohort of DCM model (n = 102 for B-mode images, n = 100 for M-mode images). Correlations between the manual user (y-axis) and the automated tool (x-axis) for ejection fraction, fractional shortening, and left ventricle systolic and diastolic volume (LVESV and LVEDV, respectively) are shown in *A*, *B*, *C*, and *G*, respectively. Ejection fraction, systolic volume (LVESV), and diastolic volume (LVEDV) were all computed from B-mode images, whereas fractional shortening was computed from M-mode images. The corresponding Bland–Altman plots are shown in *D*, *E*, *F*, and *H*, respectively. A simple linear regression line is plotted for each correlation graph, with the equation and correlation value in the *top left* corner, and a 95% CI is plotted for each Bland–Altman plot, with the bias shown in the *top left* corner. B mode, brightness-mode; CI, confidence interval; DCM, dilated cardiomyopathy; echo, echocardiography; EF, ejection fraction; FS, fractional shortening; LVEDV, LV end-diastolic volume; LVESV, LV end-systolic volume; MENN, mouse-echocardiography neural net; M mode, motion-mode.

comprehensive automated analyses. Their model achieved 97.8% accuracy in classifying 12 video views without overfitting. Ghorbani et al. (29) developed a deep learning model, EchoNet, that can accurately identify local cardiac structures and estimate cardiac function. Specifically, they have shown that EchoNet is able to measure left ventricular end-systolic volume (R^2 = 0.74), LV end-diastolic volume (R^2 = 0.70), and EF (R^2 = 0.50). Furthermore, Ouyang et al. (30) proposed a video-based deep learning algorithm, EchoNet-Dynamic, that accurately segments the left ventricle with a DSC of 0.92 and measures LVEF with a mean absolute error of 4.1%. Those applications demonstrated that the latest advances in deep learning techniques, together with increasing high-quality, annotated imaging data, can help to improve image analyses in both research and clinical practices.

Although numerous deep learning applications have been developed for analysis of echocardiograms, most are designed for use in the clinic. Echocardiography is also widely used to evaluate animal models of disease both in academic research and in drug R&D in the pharmaceutical/biotech industry, however, there is a lack of fully automated preclinical analysis applications, which would undoubtedly benefit researchers in terms of data generation rate, accuracy, and reproducibility. Damen et al. (31) used machine learning to predict left ventricular wall boundaries in murine four-dimensional (4-D) ultrasound data. In the present study, we developed a fully automated echo analysis system (i.e., MENN) for both B-mode and M-mode mouse echo data based on the U-Net architecture. This network architecture was adopted in the current work because of several advantages compared with other approaches (32–34). First, it was created specifically for biomedical image segmentation problems (17), thus no major structure modification is needed for adapting it to echo data. Second, it has exhibited great performance in a wide range of

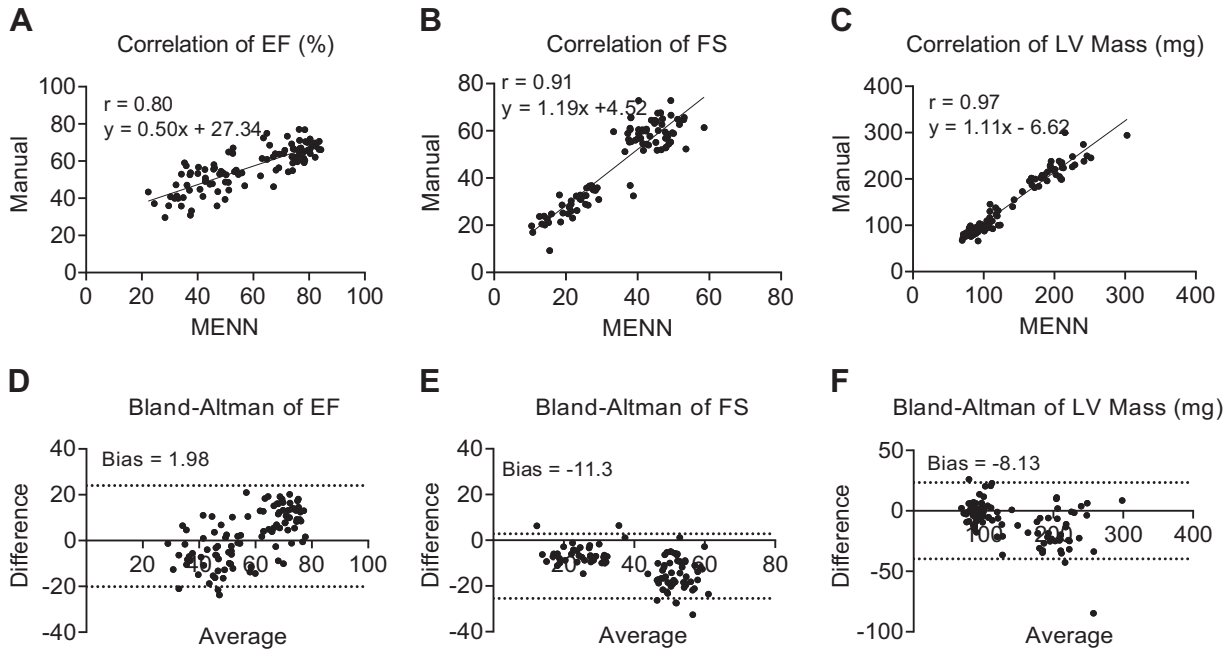

Figure 6. Performance of the mouse-echo neural net on echo images taken from the mixed cohort of HCM model (n = 103 for B-mode images; n = 98 for M-mode images). Correlations between the manual user (y-axis) and the automated tool (x-axis) for ejection fraction, fractional shortening, and corrected left ventricle (LV) mass are shown in *A*, *B*, and *C*, respectively, and the corresponding Bland–Altman plots are shown in *D*, *E*, and *F*, respectively. Ejection fraction was computed from B-mode images, whereas fractional shortening and corrected LV mass were derived from M-mode images. A simple linear regression line is plotted for each correlation graph, with the equation and correlation value in the *top left* corner, and a 95% CI is plotted for each Bland–Altman plot, with the bias shown in the *top left* corner. B mode, brightness-mode; CI, confidence interval; echo, echocardiography; EF, ejection fraction; FS, fractional shortening; HCM, hypertrophic cardiomyopathy; MENN, mouse-echocardiography neural net; M mode, motion-mode.

medical image segmentation applications (35). Third, it works with a relatively small amount of annotated training data (35). A major limitation of any deep learning technique is computational power, especially for medical image analysis where it demands performance with minimal error. The latest advances in deep learning techniques such as transfer learning (36) and EfficientNet (37) can be applied to alleviate this challenge.

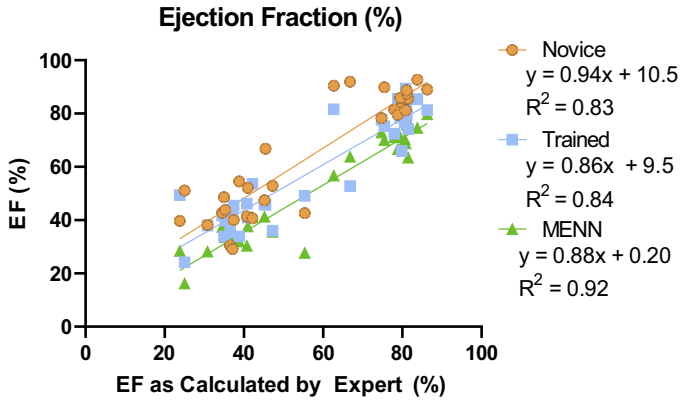

Figure 7. The mouse-echo neural net increases efficiency and reduces intrareader variability of mouse echocardiography analysis. Comparison of the estimated ejection fraction (EF) by expert (x-axis) and novice (orange), trained (blue), and MENN (green) from B-mode images (n = 30, i.e., DCM = 3, DCM plus ANG II = 12, and HCM = 15). B mode, brightness-mode; DCM, dilated cardiomyopathy; echo, echocardiography; HCM, hypertrophic cardiomyopathy; MENN, mouse-echocardiography neural net.

Although none of the existing clinical echo automation tools have been evaluated in different heart pathology conditions (12), it has been reported that the performance of preclinical semiautomated echo analysis tools depends on the pathology of heart failure models (14). For example, correlation analysis of EF between manual and Auto2DE showed Pearson's r value of −0.13 and 0.94 for a streptozotocin-induced type-1 diabetes model and a transverse aortic constriction (TAC) model, respectively (14). In contrast, the performance of the MENN tool on analyzing B- and M-mode LV images from DCM and HCM models showed a good correlation for key LV metrics between automated and manual analysis outputs. This better performance of the MENN analysis tool may be due to the fact that the tool's segmentation library has been built and trained using a large set of labeled images from a wide variety of disease models including TAC, angiotensin II-induced heart failure, and diet-induced obesity models. Although strong correlations were observed between MENN and manual analysis outputs, the Bland–Altman analysis revealed consistent negative bias on absolute values for LVESV, LVEDV, and FS during the tool performance evaluation. This may be because of a difference in the approach the tool uses to compute LV systolic and diastolic volume compared with the proprietary tool, which was used for manual analysis. The MENN analysis tool computes LV volume based on averaged maximum and minimum LV volume from a PSLAX B-mode cine loop as diastolic and systolic volumes. However, during manual analysis, the analyst identifies diastolic and systolic frames within the PSLAX cine loop, then the tool provides output based on diastolic

Table 1. *Comparing consistency and agreement of EF between expert vs. novice, expert vs. trained, and expert vs. automated analysis*

	Ejection Fraction	
	ICC (1) consistency (95% CI)	ICC (2) agreement (95% CI)
Expert vs. novice	0.86 (0.73–0.93)	0.86 (0.54–0.95)
Expert vs. trained	0.92 (0.84–0.96)	0.92 (0.84–0.96)
Expert vs. automated	0.91 (0.82–0.95)	0.91 (0.43–0.97)

Values are correlation values (95% confidence intervals); n = 30 sample size. EF, ejection fraction; ICC, intraclass correlation.

and systolic frame selection. Nevertheless, despite the negative bias on the absolute values, it should not significantly affect the evaluation of LV function in a typical longitudinal study because of the high correlations. It is worthwhile to note that the difference between disease cohorts might also be a contributing factor to the varying level of bias in different metrics (both positive and negative).

A typical preclinical echo-image acquisition workflow involves acquisition of either PSLAX LV B-mode, PSAX LV M-mode, or both. Ideally one needs an analysis tool that can perform automated analysis on both B- and M-mode images of the LV to improve analysis efficiency and reduce manual input. Although a proprietary semiautomated analysis tool (Auto2DE or AutoLV) has been developed by FUJIFILM VisualSonics to improve preclinical echo-image analysis, the tool's performance has been evaluated only on PSLAX B-mode images of rodents (14), but there is a lack of published reports on the performance of the FUJIFILM VisualSonics Vevo LAB AutoLV feature on mouse models of heart failure. Like FUJIFILM VisualSonics Vevo Lab, the latest version of VivoQuant offered a semiautomated B/M-mode segmentation module. The performance of this tool has been evaluated only on six wild-type or normal mice under control and pharmacological challenge conditions, but its performance has not been thoroughly evaluated either on dilated or hypertrophic cardiomyopathy models. Notably, both these proprietary tools require an analyst to open each individual PSLAX B-mode and PSAX M-mode images for semiautomated tracing of the LV wall (14, 16). Although these semiautomated echo analysis tools reduce the time that would otherwise be spent on manual tracing of the LV wall during B-mode image analysis, the time and manual input that is required to open each individual image to run this analysis and generate this report is still significant. In contrast, MENN is a fully automated echo analysis tool with the ability to run batch analysis on both B-mode and M-mode images of the mouse LV without requiring any manual input. Since there is no manual input required during analysis, the MENN tool saves >92% of analysis time compared with a conventional approach.

It has been widely known that echocardiography analysis in both preclinical and clinical imaging is susceptible to inter- and intraobserver variability, and that these observer variabilities vary depending on operator experience. Use of automated echo analysis tools in the clinic has significantly reduced inter- and intrareader variabilities (9, 10) and improved echo analysis. An encouraging report from Grune et al. (14) shows that the use of the Auto2DE tool reduced inter- and intraobserver variabilities in manual analysis of mouse echo images. However, the authors did not evaluate the performance of Auto2DE in relation to expert and novice analysts. EF values calculated by MENN had a stronger correlation to an expert than those calculated by a novice. In addition, performing automated analysis on the same image twice using MENN yields the same results, and therefore MENN reduces inter- and intraobserver variability in echo data analysis.

The accuracy of echo-image analysis depends on the quality of echo images as well as whether the analysis is performed manually or using an automated method (14, 38). If the echo-image quality is poor due to motion artifact or rib shadowing, it would be challenging for a manual analyst to trace the LV wall. Thus, it is not surprising to see most of the segmentation failures that occurred during MENN analysis were due to poor image quality. One of the advantages of using the MENN analysis tool is that the tool generates segmentation image files that can be reviewed for QC purposes (Supplemental Fig. S2). This feature of the tool enables an analyst to reanalyze failed images using a manual approach (~90%) or choose to exclude a given image from the analysis (~10%), depending on its quality.

Although mouse models of myocardial infarction (MI) and arrhythmia and rat models of heart failure are commonly used in preclinical research, the performance of MENN has not been evaluated on these models. The MENN tool needs to be evaluated on mouse MI models and rat heart failure models in future studies.

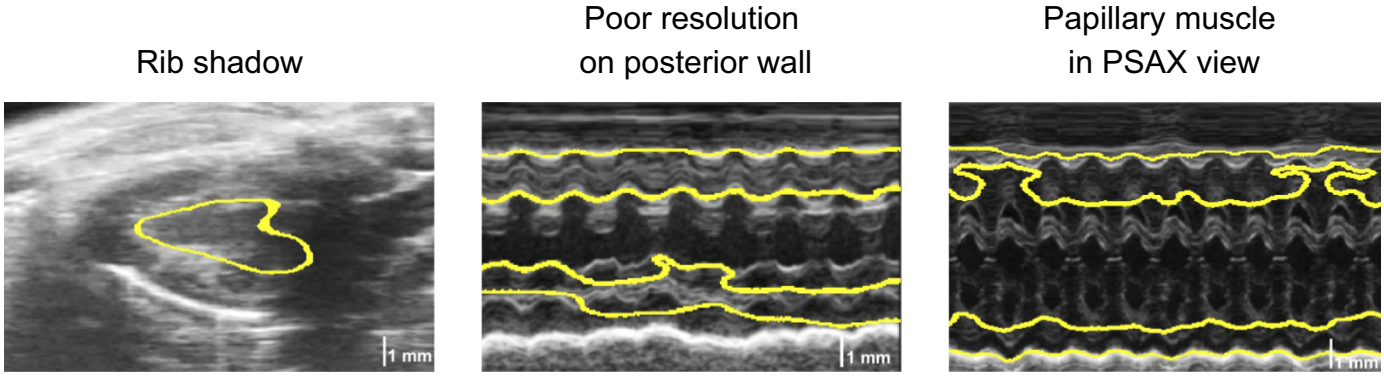

Figure 8. Examples of image quality affecting the MENN tool segmentation. MENN, mouse-echocardiography neural net; PSAX, parasternal short-axis.

In conclusion, the fully automated mouse-echo analysis tool (MENN) generates cardiac LV metrics consistent with manual analysis, reduces analysis time by more than 92%, and increases the accuracy of echo analysis by eliminating inter- and intraobserver variability.

SUPPLEMENTAL DATA

Supplemental Table S1 and Supplemental Figs. S1–S2: https://doi.org/10.6084/m9.figshare.20412552.v1.

GRANTS

This work was funded by Pfizer, Inc. (to C.D., M.K.M., X.C., S.U., J.S., K.M., D.H.-S.).

DISCLOSURES

No conflicts of interest, financial or otherwise, are declared by the authors.

AUTHOR CONTRIBUTIONS

C.D., M.K.M., and D.H.-S. conceived and designed research; C.D., M.K.M., X.C., S.U., K.M., and D.H.-S. performed experiments; C.D., M.K.M., X.C., S.U., J.S., K.M., and D.H.-S. analyzed data; C.D., M.K.M., X.C., S.U., J.S., and D.H.-S. interpreted results of experiments; C.D., M.K.M., and D.H.-S. prepared figures; C.D., M.K.M., and D.H.-S. drafted manuscript; C.D., M.K.M., X.C., S.U., and D.H.-S. edited and revised manuscript; C.D., M.K.M., X.C., S.U., J.S., K.M., and D.H.-S. approved final version of manuscript.

REFERENCES

1. **Lindsey ML**, **Kassiri Z**, **Virag JAI**, **de Castro Brás LE**, **Scherrer-Crosbie M.** Guidelines for measuring cardiac physiology in mice. *Am J Physiol Heart Circ Physiol* 314: H733–H752, 2018. doi:10.1152/ajpheart.00339.2017.
2. **Lindsey ML**, **Brunt KR**, **Kirk JA**, **Kleinbongard P**, **Calvert JW**, **de Castro Brás LE**, **DeLeon-Pennell KY**, **Del Re DP**, **Frangogiannis NG**, **Frantz S**, **Gumina RJ**, **Halade GV**, **Jones SP**, **Ritchie RH**, **Spinale FG**, **Thorp EB**, **Ripplinger CM**, **Kassiri Z.** Guidelines for in vivo mouse models of myocardial infarction. *Am J Physiol Heart Circ Physiol* 321: H1056–H1073, 2021. doi:10.1152/ajpheart.00459.2021.
3. **Paterson I**, **Mielniczuk LM**, **O'Meara E**, **So A**, **White JA.** Imaging heart failure: current and future applications. *Can J Cardiol* 29: 317–328, 2013. doi:10.1016/j.cjca.2013.01.006.
4. **Spitzer E**, **Ren B**, **Zijlstra F**, **Mieghem NMV**, **Geleijnse ML.** The role of automated 3D echocardiography for left ventricular ejection fraction assessment. *Card Fail Rev* 3: 97–101, 2017. doi:10.15420/cfr.2017:14.1.
5. **Shiota T.** 3D echocardiography: the present and the future. *J Cardiol* 52: 169–185, 2008. doi:10.1016/j.jjcc.2008.09.004.
6. **Johnson K.** Introduction to rodent cardiac imaging. *ILAR J* 49: 27–34, 2008. doi:10.1093/ilar.49.1.27.
7. **Popović ZB**, **Thomas JD.** Assessing observer variability: a user's guide. *Cardiovasc Diagn Ther* 7: 317–324, 2017. doi:10.21037/cdt.2017.03.12.
8. **Donner DG**, **Kiriazis H**, **Du XJ**, **Marwick TH**, **McMullen JR.** Improving the quality of preclinical research echocardiography: observations, training, and guidelines for measurement. *Am J Physiol Heart Circ Physiol* 315: H58–H70, 2018. doi:10.1152/ajpheart.00157.2018.
9. **Maret E**, **Brudin L**, **Lindstrom L**, **Nylander E**, **Ohlsson JL**, **Engvall JE.** Computer-assisted determination of left ventricular endocardial borders reduces variability in the echocardiographic assessment of ejection fraction. *Cardiovasc Ultrasound* 6: 55, 2008. doi:10.1186/1476-7120-6-55.
10. **Hovnanians N**, **Win T**, **Makkiya M**, **Zheng Q**, **Taub C.** Validity of automated measurement of left ventricular ejection fraction and volume using the Philips EPIQ system. *Echocardiography* 34: 1575–1583, 2017. doi:10.1111/echo.13705.
11. **Abazid RM**, **Abohamr SI**, **Smettei OA**, **Qasem MS**, **Suresh AR**, **Al Harbi MF**, **Aljaber AN**, **Al Motairy AA**, **Albiela DE**, **Almutairi BM**, **Sakr H.** Visual versus fully automated assessment of left ventricular ejection fraction. *Avicenna J Med* 8: 41–45, 2018. doi:10.4103/ajm.AJM_209_17.
12. **Cannesson M**, **Tanabe M**, **Suffoletto MS**, **McNamara DM**, **Madan S**, **Lacomis JM**, **Gorcsan J. 3rd.** A novel two-dimensional echocardiographic image analysis system using artificial intelligence-learned pattern recognition for rapid automated ejection fraction. *J Am Coll Cardiol* 49: 217–226, 2007. doi:10.1016/j.jacc.2006.08.045.
13. **Barbosa D**, **Heyde B**, **Dietenbeck T**, **Houle H**, **Friboulet D**, **Bernard O**, **D'hooge J.** Quantification of left ventricular volume and global function using a fast automated segmentation tool: validation in a clinical setting. *Int J Cardiovasc Imaging* 29: 309–316, 2013. doi:10.1007/s10554-012-0103-8.
14. **Grune J**, **Ritter D**, **Kräker K**, **Pappritz K**, **Beyhoff N**, **Schütte T**, **Ott C**, **John C**, **van Linthout S**, **Tschöpe C**, **Dechend R**, **Muller DN**, **Haase N**, **Grune T**, **Kintscher U**, **Kuebler WM.** Accurate assessment of LV function using the first automated 2D-border detection algorithm for small animals-evaluation and application to models of LV dysfunction. *Cardiovasc Ultrasound* 17: 7, 2019. doi:10.1186/s12947-019-0156-0.
15. **Howard AG**, **Zhu M**, **Chen B**, **Kalenichenko D**, **Wang W**, **Weyand T**, **Andreetto M**, **Adam H.** Mobilenets: efficient convolutional neural networks for mobile vision applications. arXiv, 2017. doi:10.48550/arXiv.1704.04861.
16. **Powers K**, **Chang R**, **Torello J**, **Silva R**, **Cadoret Y**, **Cupelo W**, **Morton L**, **Dunn M.** Development of a semi-automated segmentation tool for high frequency ultrasound image analysis of mouse echocardiograms. *Sci Rep* 11: 6559, 2021. doi:10.1038/s41598-021-85971-3.
17. **Ronneberger O**, **Fischer P**, **Brox T.** U-Net: convolutional networks for biomedical image segmentation. In: *Medical Image Computing and Computer-Assisted Intervention–MICCAI 2015*, edited by Navab N, Hornegger J, Wells W, Frangi A. Springer, Cham, Oct 5–9, 2015. vol. 9351, p. 234–241.
18. **Lessick J**, **Ghersin E**, **Abadi S**, **Yalonetsky S.** Accuracy of the long-axis area-length method for the measurement of left ventricular volumes and ejection fraction using multidetector computed tomography. *Can J Cardiol* 24: 685–689, 2008. doi:10.1016/s0828-282x(08)70666-4.
19. **Lang RM**, **Bierig M**, **Devereux RB**, **Flachskampf FA**, **Foster E**, **Pellikka PA**, **Picard MH**, **Roman MJ**, **Seward J**, **Shanewise JS**, **Solomon SD**, **Spencer KT**, **Sutton MS**, **Stewart WJ**; **Chamber Quantification Writing Group**, **American Society of Echocardiography's Guidelines and Standards Committee**, **European Association of Echocardiography.** Recommendations for chamber quantification: a report from the American Society of Echocardiography's Guidelines and Standards Committee and the Chamber Quantification Writing Group, developed in conjunction with the European Association of Echocardiography, a branch of the European Society of Cardiology. *J Am Soc Echocardiogr* 18: 1440–1463, 2005. doi:10.1016/j.echo.2005.10.005.
20. **Troy BL**, **Pombo J**, **Rackley CE.** Measurement of left ventricular wall thickness and mass by echocardiography. *Circulation* 45: 602–611, 1972. doi:10.1161/01.cir.45.3.602.
21. **Devereux RB**, **Alonso DR**, **Lutas EM**, **Gottlieb GJ**, **Campo E**, **Sachs I**, **Reichek N.** Echocardiographic assessment of left ventricular hypertrophy: comparison to necropsy findings. *Am J Cardiol* 57: 450–458, 1986. doi:10.1016/0002-9149(86)90771-x.
22. **Fang X**, **Bogomolovas J**, **Wu T**, **Zhang W**, **Liu C**, **Veevers J**, **Stroud MJ**, **Zhang Z**, **Ma X**, **Mu Y**, **Lao DH**, **Dalton ND**, **Gu Y**, **Wang C**, **Wang M**, **Liang Y**, **Lange S**, **Ouyang K**, **Peterson KL**, **Evans SM**, **Chen J.** Loss-of-function mutations in co-chaperone BAG3 destabilize small HSPs and cause cardiomyopathy. *J Clin Invest* 127: 3189–3200, 2017. doi:10.1172/JCI94310.
23. **Harris SP**, **Bartley CR**, **Hacker TA**, **McDonald KS**, **Douglas PS**, **Greaser ML**, **Powers PA**, **Moss RL.** Hypertrophic cardiomyopathy in cardiac myosin binding protein-C knockout mice. *Circ Res* 90: 594–601, 2002. doi:10.1161/01.res.0000012222.70819.64.

24. **Shen D**, **Wu G**, **Suk HI.** Deep learning in medical image analysis. *Annu Rev Biomed Eng* 19: 221–248, 2017. doi:10.1146/annurev-bioeng-071516-044442.
25. **Litjens G**, **Ciompi F**, **Wolterink JM**, **de Vos BD**, **Leiner T**, **Teuwen J**, **Išgum I.** State-of-the-art deep learning in cardiovascular image analysis. *JACC Cardiovasc Imaging* 12: 1549–1565, 2019. doi:10.1016/j.jcmg.2019.06.009.
26. **Litjens G**, **Kooi T**, **Bejnordi BE**, **Setio AAA**, **Ciompi F**, **Ghafoorian M**, **van der Laak J**, **van Ginneken B**, **Sánchez CI.** A survey on deep learning in medical image analysis. *Med Image Anal* 42: 60–88, 2017. doi:10.1016/j.media.2017.07.005.
27. **Klose AD**, **Paragas N.** Automated quantification of bioluminescence images. *Nat Commun* 9: 4262, 2018. doi:10.1038/s41467-018-06288-w.
28. **Madani A**, **Arnaout R**, **Mofrad M**, **Arnaout R.** Fast and accurate view classification of echocardiograms using deep learning. *NPJ Digit Med* 1: 6, 2018. doi:10.1038/s41746-017-0013-1.
29. **Ghorbani A**, **Ouyang D**, **Abid A**, **He B**, **Chen JH**, **Harrington RA**, **Liang DH**, **Ashley EA**, **Zou JY.** Deep learning interpretation of echocardiograms. *NPJ Digit Med* 3: 10, 2020. doi:10.1038/s41746-019-0216-8.
30. **Ouyang D**, **He B**, **Ghorbani A**, **Yuan N**, **Ebinger J**, **Langlotz CP**, **Heidenreich PA**, **Harrington RA**, **Liang DH**, **Ashley EA**, **Zou JY.** Video-based AI for beat-to-beat assessment of cardiac function. *Nature* 580: 252–256, 2020. doi:10.1038/s41586-020-2145-8.
31. **Damen FW**, **Newton DT**, **Lin G**, **Goergen CJ.** Machine learning driven contouring of high-frequency four-dimensional cardiac ultrasound data. *Appl Sci (Basel)* 11: 1690, 2021. doi:10.3390/app11041690.
32. **Ciresan D**, **Giusti A**, **Gambardella L**, **Schmidhuber J.** Deep neural networks segment neuronal membranes in electron microscopy images. *Proceedings of the 25th International Conference on Neural Information Processing Systems—(NIPS'12)*. Red Hook, NY, Dec 3, 2012, vol. 2, p. 2843–2851
33. **Seyedhosseini M**, **Sajjadi M**, **Tasdizen T.** Image segmentation with cascaded hierarchical models and logistic disjunctive normal networks. *Proc IEEE Int Conf Comput Vis* 2013: 2168–2175, 2013. doi:10.1109/ICCV.2013.269.
34. **Long J**, **Shelhamer E**, **Darrell T.** Fully convolutional networks for semantic segmentation. *Proc IEEE Conf Comput Vis and Pattern Recognition* 3431–3440, 2015. doi:10.1109/CVPR.2015.7298965.
35. **Siddique N**, **Paheding S**, **Elkin CP**, **Devabhaktuni V.** U-net and its variants for medical image segmentation: a review of theory and applications. *IEEE Access* 9: 82031–82057, 2021. doi:10.1109/ACCESS.2021.3086020.
36. **Frid-Adar M**, **Ben-Cohen A**, **Amer R**, **Greenspan H.** Improving the segmentation of anatomical structures in chest radiographs using u-net with an imagenet pre-trained encoder. In: *Image Analysis for Moving Organ, Breast, and Thoracic Images*. Cham, Switzerland: Springer, 2018, p. 159–168.
37. **Tan M**, **Le Q.** Efficientnet: Rethinking model scaling for convolutional neural networks. *Proceedings of the 36th International Conference on Machine LearningPMLR*. 2019, p. 6105–6114.
38. **Nagata Y**, **Kado Y**, **Onoue T**, **Otani K**, **Nakazono A**, **Otsuji Y**, **Takeuchi M.** Impact of image quality on reliability of the measurements of left ventricular systolic function and global longitudinal strain in 2D echocardiography. *Echo Res Pract* 5: 27–39, 2018. doi:10.1530/ERP-17-0047.